https://doi.org/10.61092/iaea.4z3d-bbpm

INDC(NDS)-0839
Distr. G,NM,PH

IAEA
International Atomic Energy Agency

INDC International Nuclear Data Committee

The E1 and M1 UPBEND in Neutron Capture Revisited

J. Kopecky
JUKO Research
Alkmaar, The Netherlands

S. Goriely
Université Libre de Bruxelles,
Brussels, Belgium

March 2022

IAEA Nuclear Data Section
Vienna International Centre, P.O. Box 100, 1400 Vienna, Austria

Selected INDC documents may be downloaded in electronic form from
http://nds.iaea.org/publications
or sent as an e-mail attachment.
Requests for hardcopy or e-mail transmittal should be directed to
NDS.Contact-Point@iaea.org
or to:
Nuclear Data Section
International Atomic Energy Agency
Vienna International Centre
PO Box 100
1400 Vienna
Austria

Printed by the IAEA in Austria

March 2022

INDC(NDS)-0839
Distr. G,NM,PH

The E1 and M1 UPBEND in Neutron Capture Revisited

J. Kopecky
JUKO Research
Alkmaar, The Netherlands

S. Goriely
Université Libre de Bruxelles,
Brussels, Belgium

March 2022

Contents

1. Introduction

The upbend phenomenological modelling has been introduced in Refs. [1,2] and described by Eqs. 1 and 2 in Ref. [1]. Both, the constant E1 upbend and the increasing M1 upbend with decreasing E_γ are based on the shell model calculations of light nuclei which have guided the shape of these phenomenological expressions [1]. The Oslo data have been used to determine an adjustment to the experiment results. These data, however, include the E1 plus M1 modes, which may be a source (their ratio) of the uncertainty together with the level density model dependency used in their derivation. Furthermore, the Oslo data do not extend below a gamma ray energy of 2 MeV, thus the lowest energy region is missing. Such a situation certainly shows the need to search for additional reliable data, especially for energies below 2 MeV.

The neutron capture with energies above the thermal region, such as the discrete resonance capture (DRC) or average resonance capture (ARC) data, suffer from the fact that the low energy data are not measured, and this for two reasons. The energy cutoff of the gamma-ray pair spectrometers is at 3-4 MeV and if the single Ge (Li) low-energy data are measured, their large amount complicates the assignment of the primary mode. This means that for the DRC and/or ARC measurements the low energy detection limit is around 4 MeV and consequently no direct information for the upbend region is available.

However, the thermal capture (THC) technique, not yet fully exploited in photon strength function (PSF) studies, is certainly an important source of information, with its high quality of low-energy data, especially for light mass targets due to their low level densities. The recently evaluated THC data over several transitions [3-5] give a quite robust information on the low-energy primary transisitions and their strength behaviour. Another source of THC data is collected in the EGAF database [6], which includes a complilation of data from targets within the mass region $6 < A < 240$. The results are given in a binned (over several transitions) format to diminish the strong Porter/Thomas fluctuations.

In this work we concentrate on the thermal data and seek for new evidence for the upbend behavior, in combination with the averaged data. The strong low-energy gamma rays that have been detected in light mass targets have not yet been used to learn about the E1 upbend formalism [1]. The situation is shown in Fig. 1 for nuclides with $A < 60$. The THC data, binned over the E_γ region of 0.5 – 2 MeV, are plotted with the EGAF data entries below $\langle E_\gamma \rangle = 2.5$ MeV.

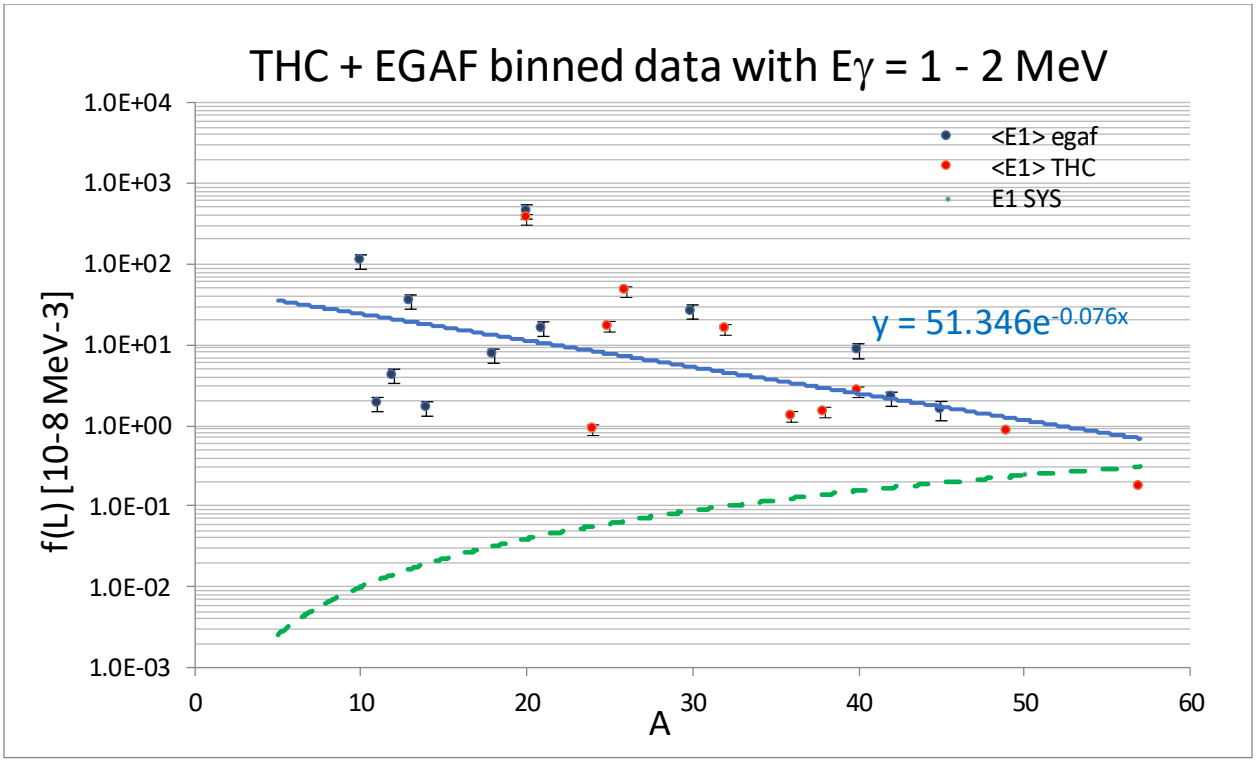

FIG. 1. PSF data from THC data [4] and EGAF thermal capture data [6] plotted as function of the mass A. The data with energies between 0.5 – 2.5 MeV (majority within 1 and 2 MeV) have been used as entries. The common trend follows the exponential dependence of ~ $e^{-0.07A}$ increasing with $A \rightarrow 0$. The <6.5 MeV> systematic is plotted (green dashed line) to show the excess of PSF experimental values against the tail of the statistical Giant Dipole Resonance (GDR) prediction. This situation is supported by Fig. 25 in Ref. [2].

The present work has been carried out with the aim to investigate the E1 and M1 THC data and the underlying modelling of low-energy transitions with $E_\gamma \rightarrow 0$. This report is divided in two main sections, studying E1 and M1 behavior at low gamma-ray energies. We have chosen the mass range with $A < 70$, one of the reasons is that in this mass region the ARC data are absent and the DRC data are scarce and based on a limited amount of resonances. We will concentrate on possible new information on the PSF behavior in the upbend region for E1 and M1 strength separately, and try to compare and connect the low energy results with previous ARC/DRC observations for $A > 70$. The final section will give conclusions and ideas for novel revisions of the upbend expressions.

2. E1 radiation

2.1. Low mass targets: the ^{28}Al case and validation test analysis

This subsection is devoted to test processing and assumptions in the analysis of thermal capture data used for the PSF conclusions. The light target ^{27}Al has been chosen. The present situation of the ^{28}Al THC data and the theoretical predictions of the D1M+QRPA+0lim and shell model (SM) calculations are shown in Fig. 2 (taken from Refs [1,3]).

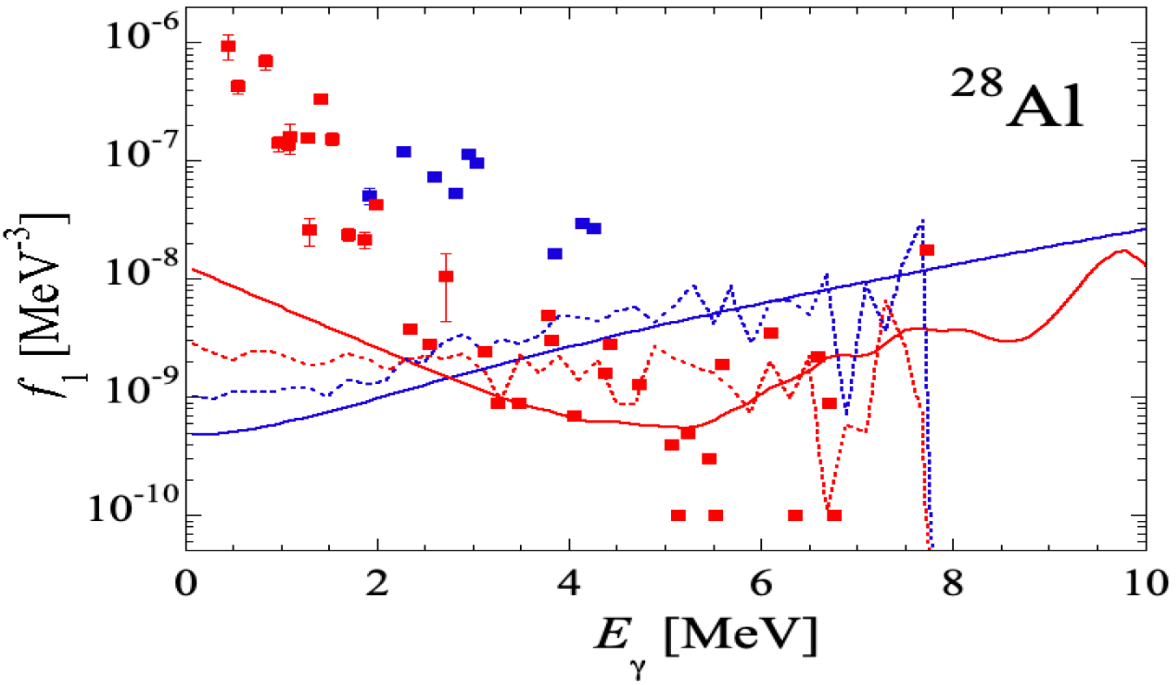

FIG. 2. THC E1 (blue) and M1(red) data plotted together with D1M+QRPA+0lim *prediction (full curves) and the SM results (dotted curves). Note the underestimation of the E1 experimental PSF below $E_\gamma \simeq 4$ MeV by both theoretical predictions, while the M1 prediction starts to disagree below 3 MeV. Further note the almost constancy of the SM curves at the lowest energies which indicates that the gamma-ray energy dependence is close to E_γ^3 for both E1 and M1 radiation.*

In this section we further concentrate on E1 radiation only. The first action was to check the absolute normalization of the intensity I_γ and this was done by a comparison of two independent thermal data experiments, the analysis in Refs. [3-5] and the EGAF data [6]. The results are shown in Fig.3 where data are derived from the original analysis of Ref. [8] and compared with a re-analysis with recent spectroscopic information.

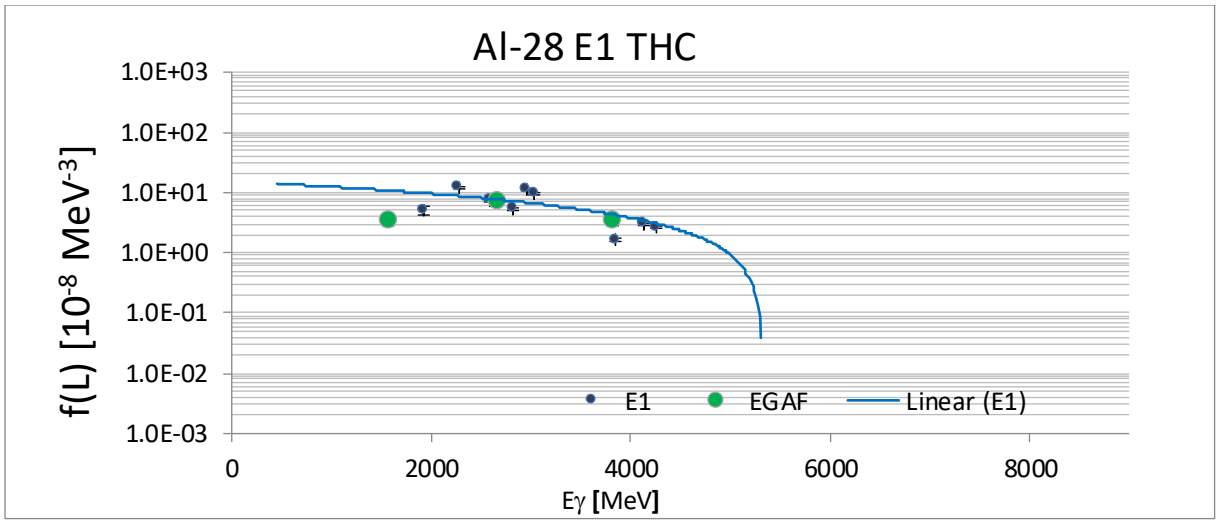

FIG. 3. THC data from Ref. [3] and the EGAF binned database [6]. Note the good agreement between two independent data sets; this supports the absolute calibration together with the total strength which obeys $\Sigma I_\gamma \simeq 100$ and indicates that the majority of primary strength is assigned in the decay scheme.

The other comparison was against the resonance data. The only DRC experiment for the ^{27}Al target is the fast neutron capture measurement of Bergqvist [8]. The data adopted in the DRC include three resonances at E_n = 34.8keV ($J = 3^+$), 86.2 keV (2^+) and 91.4 keV (3^-). A search for possible unresolved doublets has been carried out because of the use of NaI total-absorption spectrometer with limited gamma-ray resolution. After a careful treatment we have decided to use only the data from the lowest s-wave resonance at 34.8 keV.

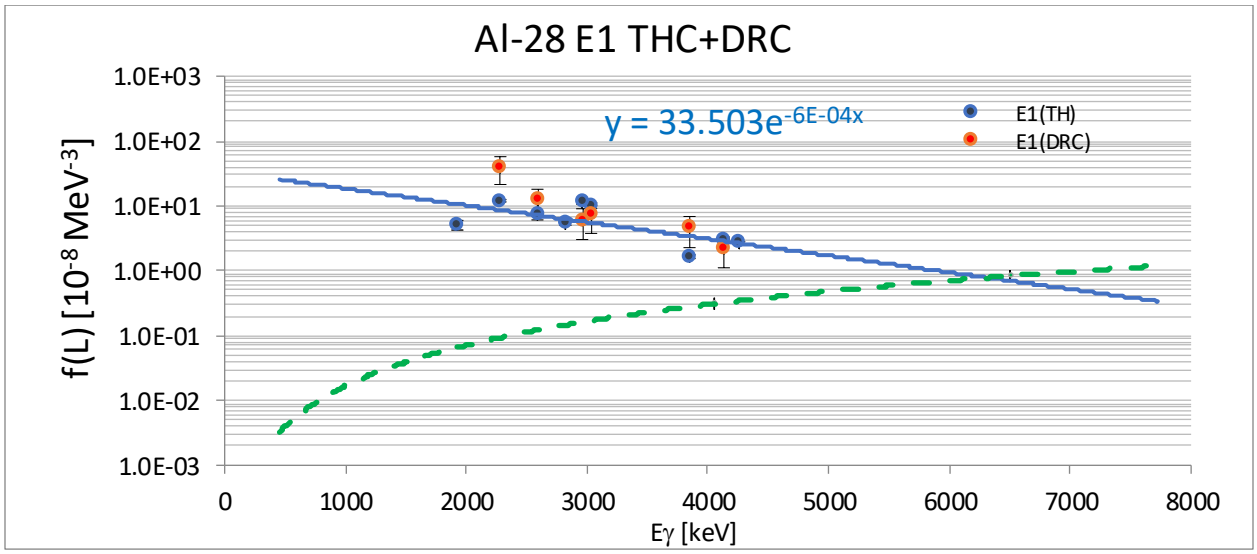

FIG. 4. E1 THC data from the ^{27}Al(n,γ) reaction and the DRC data from the 34.8 keV s-wave resonance together with the systematic <<f(E1)>>(6.5MeV) curve (green dashed line). Note the good agreement of the THC and DRC data.

The statistical quality of I_γ intensities of the second resonance was found insufficient and the third p-wave resonance was only quoted in an integral decay strength. The results of the new DRC ^{28}Al data are shown in Fig. 4. The authors in Ref. [8] have reached the following conclusion which may be relevant for the use of the combined E1 and M1 experimental data as Oslo measurements:

> "The keV capture experiments, in good agreement with those of other nuclides in this mass region, establishing with no outstanding exceptions, that M1 competes favorably with E1. An empirical rule, valid at least for neutrons of keV energy and lower, seems to operate in the case of the s−d-shell nuclides."

The low-energy E1 data for ^{28}Al indicate a good agreement between THC and DRC experiments and the disagreement between the experimental data and the D1M + QRPA +0lim prediction in Fig. 2. Another obvious possible contribution to the E1 strength upbend for ^{28}Al comes from the Direct Capture (DC) model (reviewed in Refs [4,5]) and discussed in Section 2.2.

The recent upbend treatment in ^{28}Al - The D1M+QRPA+0lim results in Fig. 2 used the phenomenological E1 upbend expression (Ref [1]) given by

$$f_{E1}(E_\gamma) = f_{E1}^{QRPA}(E_\gamma) + f_0 U / [1 + e^{(E_\gamma - E_0)}], \quad (1)$$

of the initial de-exciting state and f_0 and E_0 are free parameters adjusted to the SM calculations or the Oslo data (Ref [1]). The E1 upbend is assumed, in all E1 decays, independent of the deformation. The upbend component is negligibly dependent on the gamma-ray energy below the neutron binding energy B_n. The D1M+QRPA+0lim PSF, including the upbend (for an excitation energy U = 5 MeV), is compared in Fig. 6 for ^{28}Al with the THC experimental data (Ref [8]).

The fitted curves are smooth eye-guiding trend fits of the data entries. The difference between the experimental data and the theoretical prediction (red curves) is enormous and the upbend component (blue constant curve in Fig. 5, left panel) is unable to solve the disagreement. The size needed for a reasonable fit is impossible to be viewed as a "constant background" contribution and an energy dependent component, increasing with the decreasing E_γ, needs to be proposed. The gamma ray strength function definition requires a phase reduction of the dipole radiation by a factor of E_γ^3. This means that when we try to identify the E_γ dependence of the PSF, firstly we "reduce" the absolute gamma strength I_γ or $\Gamma_{\gamma i}$ by this factor. Any deviation from this dependence suggests the relevance of a model with another energy dependence. In the ARC (2 and 24 keV capture) measurements the I_γ/E_γ^5 ratio was successfully used as a tool to identify the E1 primary transitions, based on the assumption that the GDR model ($\sim E_\gamma^5$) dominates the decay. This dependence has been confirmed in the whole mass region for $E_\gamma > 4$ MeV transitions, leading to the E_γ^2 PSF dependence (Refs [1-5, 9-11]). The PSF data above 4 MeV follow several GDR models and are further in agreement with the theoretical D1M+QRPA. However, for $E_\gamma \rightarrow 0$ the standard Lorentzian (SLO) and the D1M+QRPA models tend to zero in disagreement with experimental evidence.

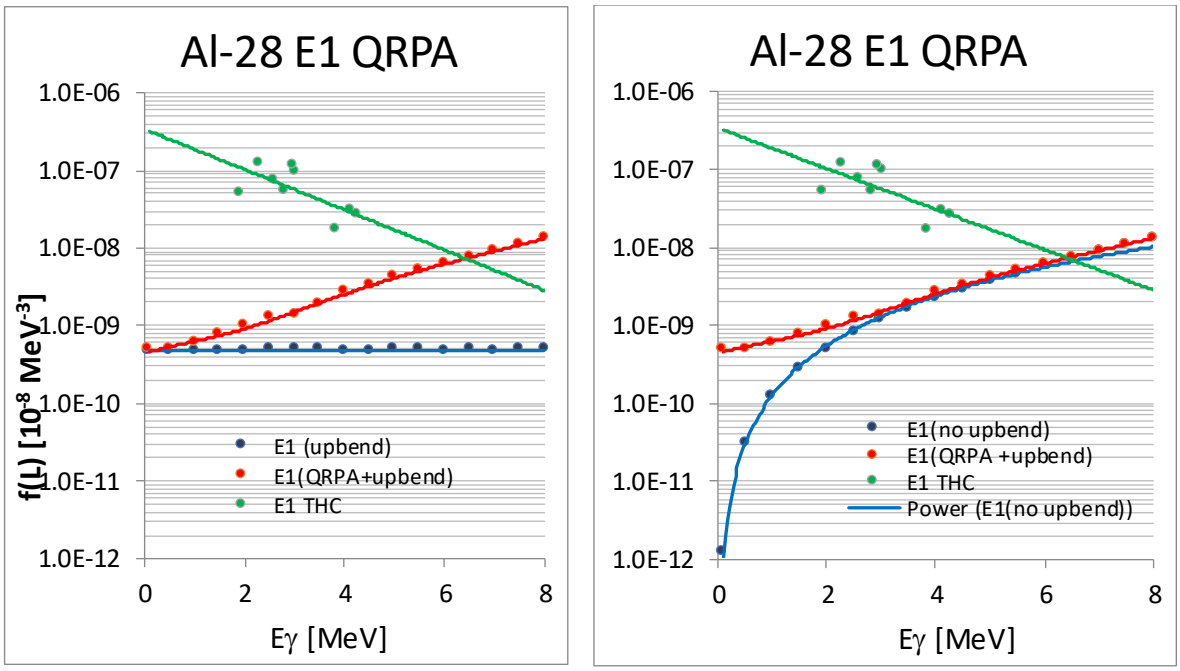

FIG. 5. THC data compared with the theoretical predictions of the D1M+QRPA and upbend components. Note the constancy and small contribution of the upbend with U = 5 MeV and large disagreement of the pure statistical contribution from the D1M+QRPA model, which reproduces the PSF E1 data (ARC, DRC, THC) for energies above 4 MeV.

Several Lorentzian based models (GLO, EGLO and MLO) have been proposed to solve this problem by introducing a dependence with respect to the final state nuclear temperature *T*. The role of nonstatistical effects such as the DC has already been discussed in Refs [3-5], therefore it seems to be evident that the DC may significantly contribute and even dominate for certain mass regions.

The trend analysis, recently introduced in Refs [4,5], crudely infers the energy dependence of experimental data by a fitted trend function. If the power dependence is applied, the fitted slope can be used to guess the underlying "model" energy dependence. The slope analysis has been used earlier and details can be found in Refs [4,5]. If we assume that the DC component is responsible for the E1 strength in ^{28}Al, we can expect the PSF phase space factor to vary as E_γ^{-2}. The slope of the E1 THC data was found as $E_\gamma^{-1.7}$ which agrees rather well with the expected DC model (Ref. [12]), taking all uncertainties into account. This suggests that the nonstatistical influence in the 2s1d-shell targets is present and should be taken into account for all targets. The analysis of the data trend uses an exponential dependence which better describes the dependence in a broader region and is less sensitive to a singular outlier. Such a trend analysis will be used to predict the E1 PSF limit at $E_\gamma = 0$.

The major uncertainty of the trend analysis at low energies, besides the width of the adopted energy range, can be the effect of missed points especially below $E_\gamma \sim 1$ MeV. Data in this energy region are rarely measured or identified as primary transitions. To test the influence of these missing transitions, two measurements of ^{33}S from McMaster University (Ref. [13]) and Raman et al. (Ref. [14]) have been compared. While the lowest detected E1 transition in Ref. [16] has the energy E_γ = 1965 keV, five transitions in Ref. [15] have been identified below this energy with the lowest

at E_γ = 274 keV. Both derived PSFs are shown in Fig. 6. The results show that the trend of data in the E_γ range between 2 and 5 MeV, dominant for the slope exponent value, is not severely influenced by the data below 1 MeV. Encouraged by this result we expect that the trend analysis is a tool which can help to identify the PSF value at E_γ = 0.

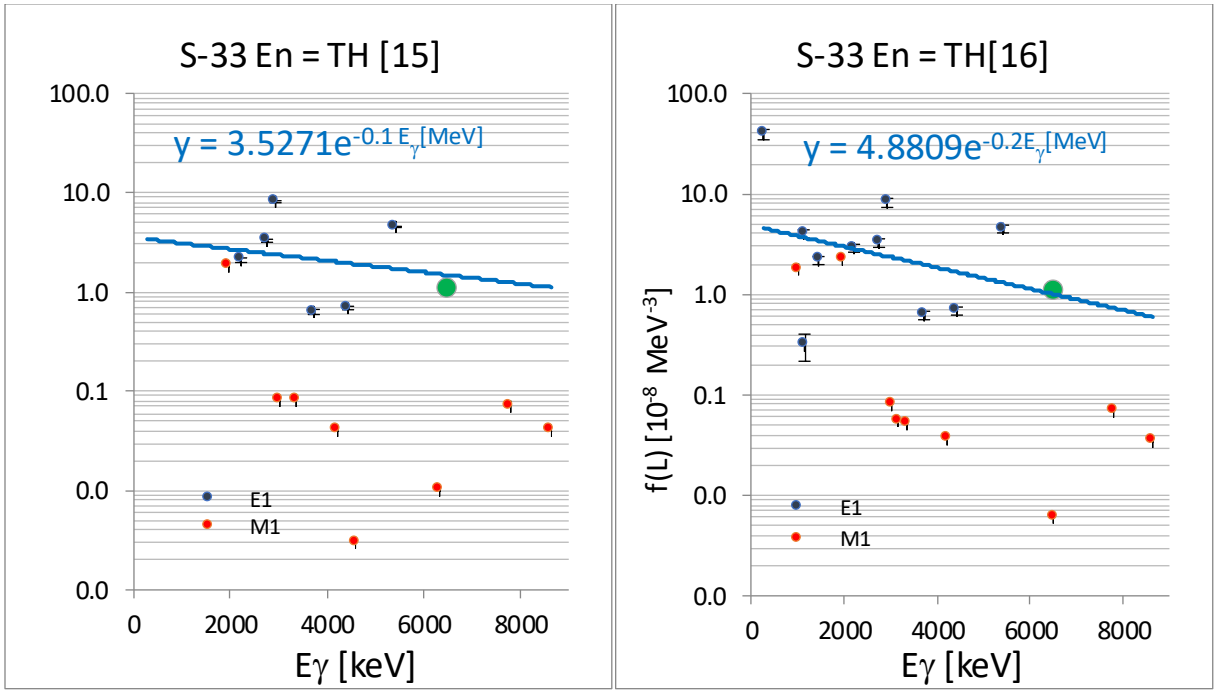

FIG. 6. Differential PSF values of primary transitions in ^{33}S, derived from I_γ intensities from Refs [15] and [16], for final states with unambiguously assigned parity that guarantees the E1 and M1 selection. The green data point is the <f(E1)> systematics at 6.5 MeV. Plotted curves are unweighted trend fits to show the PSF behavior as an exponential function of E_γ and used in the trend analysis. Note the small difference in the power exponent of both E1 curves and the similarity of data above 2 MeV.

The main conclusion here supports the present THC analysis and suggests that it can be safely applied to the remaining light mass targets to study their low-energy data behavior.

2.2. Direct capture

The ^{28}Al thermal cross section analysis, based on parameters from Ref. [17], fully supports the DC origin of E1 transitions: $\sigma(\gamma)_{th}$ = 0.231 b, $\Sigma I_\gamma(E1)$ = 0.48 => $\sigma(E1)$ = 0.111b and the calculated $\sigma(DC)$ = 0.108. The presence of the non-statistical mode is further supported by a strong (n,γ)-(d,p) correlation (a well-established signature for the DC model) found in Refs [13,16]. Based on this result we may expect that DC gives a dominant contribution to the gamma-ray E1 strength extracted in light s-d shell targets. Its strength and the region of influence can be estimated from the calculated DC contributions (Ref. [17]) to the thermal capture (see Refs [4,5]), as shown in Fig. 7. One question remains open, namely how the GDR model functions in the 3s –> 2p(1f) shell configuration and to what extent the E1 systematics is applicable in these nuclides if the E1 energy is far from 6.5 MeV.

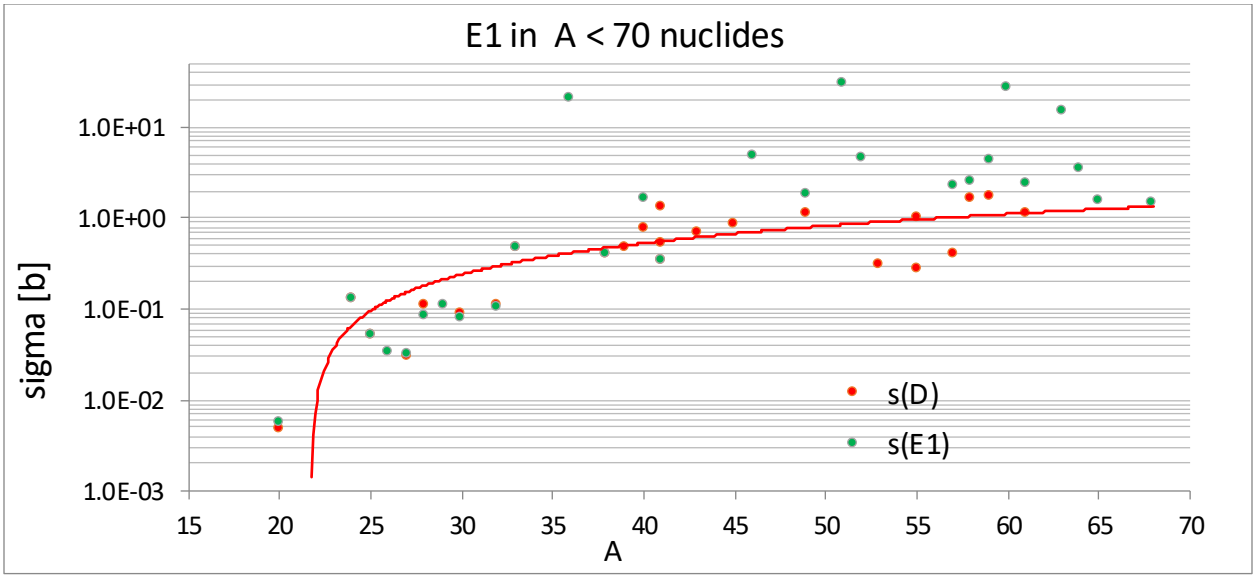

FIG. 7. Thermal E1 cross sections derived from Ref. [17] (σ(E1) green points) plotted together with the calculated DC component [17] (σ(D) red points) for targets with A < 70. The plotted curve is a fitted trend only for visual guidance. Note that for several nuclides with A < 35 both values are equal. The two strong data points above 10b belong to single resonance thermal cross sections of ^{35}Cl and ^{50}V. The behavior for targets above A ~ 50 suggests that the statistical mode starts to dominate. It may be concluded that the E1 strength for light mass targets with A < 45 is dominated by the DC model providing the major E1 component and overruling the standard upbend.

The THC state, i.e., the initial state for the THC, especially for light nuclides is formed by tails of positive/negative resonances and/or the potential capture. As mentioned in Ref. [17]:

> "The direct capture cross section σ_γ(D) is calculated for 2200 m/s neutrons in the framework of the Lane-Lynn theory. This was done to differentiate the contribution from the negative energy resonances (called the bound states) and the direct capture component. It is assumed here that interference terms between the direct and the compound components are absent or negligible. Because of the absence of nearby s-wave resonances in some nuclei, the internal compound resonance contribution is negligible, resulting in σ_γ (B) = σ_γ (D)."

This results in the resonance tails between resonances being negligible and not affecting the cross section (the area of DRC and ARC data). This implies that they differ fundamentally from the thermal capture state and, furthermore, that the Brink hypothesis is not applicable for general PSF conclusions.

The present analysis can be finalized with the following conclusions:

1. The presence of the nonstatistical direct capture in the thermal capture for $A < 70$ targets is confirmed, based on a robust analysis of experimental THC and EGAF results, using a large number of primary transitions with $1 < E_\gamma < 4$ MeV.
2. This effect is dominant for targets below $A \sim 45$ while for masses up to $A \sim 70$ the GDR model starts to dominate the E1 strength due to the shift of the 2p(1f) shell to lower excitation energies and by depopulating E1 primary transitions with energies above 5 MeV. The experimental data below 4 MeV are then absent.

3. In targets, where the DC dominates (light nuclides), the statistical GDR model is at low E_γ energies (0lim region) dominated by the DC contribution
4. However, it needs to be kept in mind that this effect is present only for thermal neutron incident energies and should not be included in general E1 description.
5. THC data for A<45 nuclei are affected by the dominant DC component and should therefore not be considered to extract a statistical PSF at low energy.

2.3. THC database for A < 70 nuclides

Based on results and experience with the ^{28}Al data processing, this methodology is applied to all A < 70 targets to search for either possible systematic behavior or the origin of low-E_γ transitions. We have addressed all measured targets (compared with the EGAF listing) below A ~ 70 and generated a new database called *E1THC70* (Ref. [18]). As data sources we used the present THC evaluations or the EGAF partial E_γ/I_γ data. The choice of the adopted source was based on a comparison of both entry libraries. The EGAF data have been adopted only if they were superior to THC data or if the latter were absent. The final list is given in Table 1. Data with transitions only above E_γ = 4 MeV have not been included.

TABLE 1. List of recommended E1 thermal capture data with A < 70 from the THC and EGAF data sources. The last column gives the 0lim exponential intercept of the PSF at E_γ =0, derived from E_γ < 4 MeV data points. No entry is given for disregarded trend (data shortage) or missing data below 4 MeV. For a detail overview, it is recommended to download data from the *E1THC70* link.

EGAF/PGAA	**THC**	**EGAF** processed in this work	**Recommended sources**	**Trend** DC + 0lim for visual analysis	**Trend** 0lim for visual analysis	$f_{E1}(E_\gamma = 0)$ [10^{-8}MeV^{-3}]
F-20	+		THC			
Na-24	+		THC	+		2.74
Mg-25	+		THC	+		16.57
Mg-26	+	+	THC+ EGAF			
Mg-27	+		THC			73.59
Al-28	+		THC	+		33.50
Si-29	+	+	EGAF	+		4.33
Si-30	+	+	EGAF	+		21.84
P-32	+		THC	+		11.36
S-33	+	+	EGAF	+		15.57
S-34	+	+	THC+ EGAF	+		10.8
S-35	+		THC	+		2.40
Cl-36	+		THC	+		11.3
Cl-38	+		THC	+		4.86
K-40	+		THC	+		2.36
Ar-41		+	EGAF	+		7.59
K-41		+	Not used			
Ca-41	+		THC			
K-42		+	EGAF	+		14.44
Ca-44		+	EGAF			
Ca-45		+	EGAF	+		2.22
Sc-46	+		THC			

EGAF/PGAA	**THC**	**EGAF** processed in this work	**Recommended sources**	**Trend** DC + 0lim for visual analysis	**Trend** 0lim for visual analysis	$f_{E1}(E_\gamma = 0)$ [10^{-8}MeV^{-3}]
Ti-49	+		THC		+	0.41
Ti-50		+	EGAF			
V-51	+		THC			
Cr-51	+		THC			
V-52	+		THC			
Cr-55		+	EGAF			
Mn-56		+	EGAF		+	1.6
Fe-57	+		THC		+	0.23
Fe-59		+	EGAF			0.07
Ni-59	+		EGAF		+	
Co-60	+	+	THC+ EGAF			
Ni-61	+	+	THC+ EGAF			1.80
Ni-63	+	+	EGAF			0.19
Cu-64	+		THC			1.67
Ni-65		+	EGAF			
Zn-65	+		THC			
Cu-66	+		THC			0.38
Zn-68	+		THC			

For all recommended sources (see the 4th column) a graphical presentation has been prepared. The assigned E1 entries are divided into two groups, those with $E_\gamma < 4$ MeV and data above 4 MeV. This division assumes that the statistical contribution below 4 MeV is small and that the low-energy data give primarily an information on the "upbend" component which substantially differs from the statistical $E_\gamma \rightarrow 0$ imit. An example of such a graphical approach is shown in Fig. 8 for ^{38}Cl data. The <<6.5 MeV>> systematics is added to indicate the expected performance of the statistical model. For the trend curve, an exponential format is used; this allows to extrapolate the PSF closed to the $E_э = 0$ limit. The uncertainty of such a trend prediction is given by the size and width of the E1 data points "window" below 4 MeV.

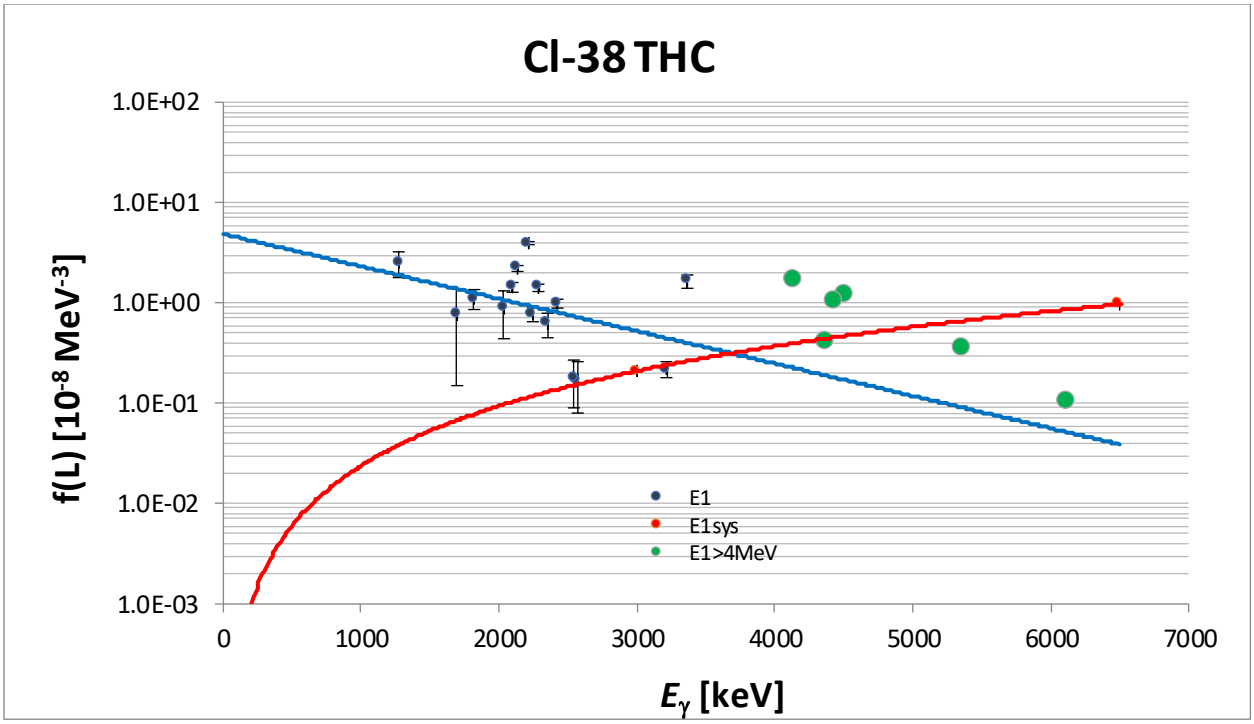

FIG. 8. E1 PSF data of ^{37}Cl(n,γ)^{38}Cl reaction plotted for the trend analysis of the upbend 0lim performance. The red curve is a GDR estimate based on the DRC <<6.5 MeV>> systematics.

In the conclusion for targets with $A < 45$ (Section 2.2.), the competition between the DC contribution and the tail of the statistical model has been acknowledged. Two columns in Table 1 show values, which can be used to visually differentiate both upbend components.

The adopted trend projections of data are given in the last column of Table 1 and plotted in Fig. 9. The resulting $E_\gamma = 0$ values are affected by uncertainties due to differences in the number of data points, their amount and E_γ energies. However, uncertainties are small enough not to disturb the median of the data. The above-mentioned competition of two different upbend components is nicely demonstrated by the difference of the $f_{E1}(E_\gamma = 0) = 14.8$ and $0.79\ 10^{-8}$ MeV^{-3} for the DC and statistical modes, respectively. From this ratio, it is obvious that the statistical upbend component is negligible for nuclides where the DC is active. For data with $A > 50$, the number of pure 0lim entries is limited and for more information on the 0lim region, estimates should be looked for in heavier nuclides (see the following section).

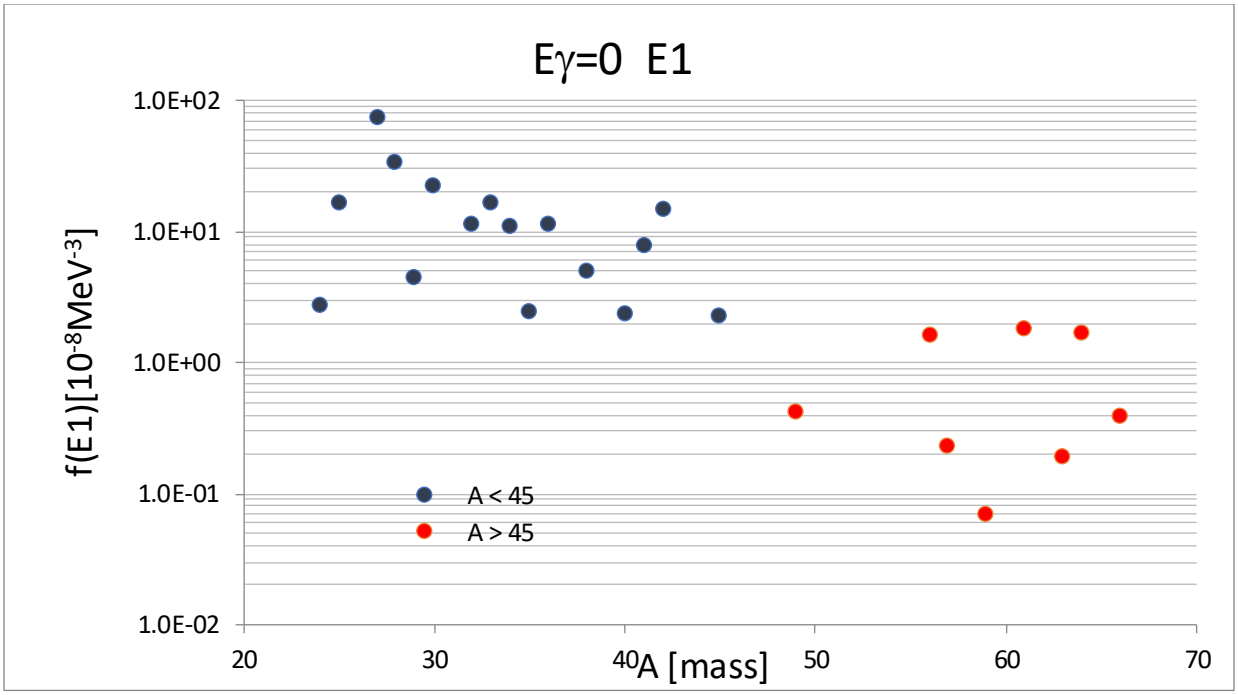

FIG. 9. Adopted $E_\gamma = 0$ PSF from the exponential trend analysis of the E1 THC data for targets with $A < 70$. Note the distinct difference between the two mass regions above and below A~45.

2.4. Binned PSF data from A > 70 nuclides

The shift of primary E1 transitions to higher E_γ energies has been observed in the previous section for nuclides with $A > 50$. This is common to all PSF data, including thermal (THC) and average resonance (DRC and ARC) capture data. The Brink hypothesis (Ref. [19]) has become a tool to describe the E1 emission in Lorentzian-based models starting with the standard Lorentzian (SLO) model with an energy-independent width Γ_r. However, severe problems of this model have been identified, such as the overestimation of the E1 strength below the binding energy and/or the underestimation of the gamma-ray spectra at low E_γ energies. Especially the disagreement in the gamma-ray spectra suggested a possible underestimation of the E1 strength at low energies. To overcome these problems, Kadmenskij et al. (Ref. [20]) proposed an energy dependence GDR width and a temperature broadening of final states which led to a E1 PSF with a non-zero low-energy limit. These problems have been addressed with success by different GDR models, such as GLO (Refs [21-23]), EGLO (Ref. [24]) and SMLO (Refs [25,26]) models and recently by the microscopic D1M+QRPA+0lim calculations (Refs [1,2]). The high energy PSF values ($E_\gamma > 4$ MeV) have been successfully validated up to the actinide region, however, the low-energy E1 transitions (for $E_\gamma < 4$ MeV) have not been sufficiently analyzed and thus the PSF behavior for E_γ approaching zero energy remained open. The absence of such transitions has two reasons. Firstly, the presence or absence of proper initial and final states severely influences the location of the E1 strength in the decay scheme and, consequently, the available experimental information. The other limitation is due to the low detection efficiency of the Ge (Li) pair spectrometry for low-E_γ energies. Additionally, the decreased resolution power of the single crystal Ge (Li) detectors at low energies with increased number of secondary transitions below $E_\gamma < 4$ makes the assignment of primary transitions difficult.

Until now we have primarily explored the partial THC data with $A < 70$, but for heavier nuclides the data below $E_\gamma \sim 4$ MeV are missing. That was the reason to turn our attention to another THC source, namely the binned EGAF data. The full information on the binned (over several entries in an energy window) EGAF database is given in Ref. [2]. The large amount of data is presented in Figs 24 and 25 of Ref. [2] where it is compared with the SMLO and D1M+QRPA+0lim predictions as a function of the mass A and the energy E_γ. However, this global comparison smooths away the behavior of individual nuclides. We have chosen another approach to the binned EGAF data from Ref. [6] (a robust thermal capture database) and the result is shown in Fig. 10.

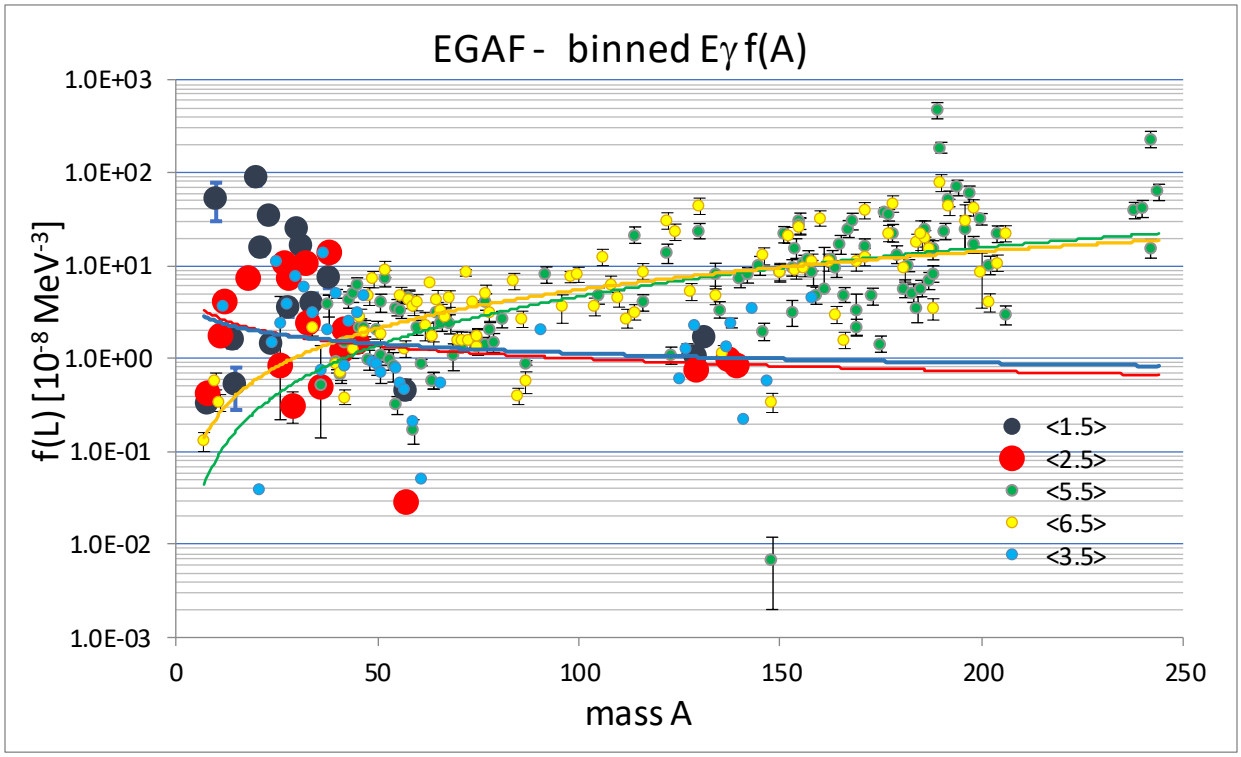

FIG. 10. Grouped EGAF data plotted as a function of the mass A. The average energy groups <E_γ> are given in the right corner. The plotted trend curves serve as a guiding average. Data below 3 MeV are plotted as the large data points to indicate their presence only for targets below A ~ 70. The extended three points at A ~ 130 are exceptions. However, in this region, with the DC 3s –> 2p(1f) shell configuration, a significant DC component is again expected. Going to higher energy groups the trend is nicely changing to an A^5 dependence, as expected from the GDR model.

To get a partially unsmoothed response on the mass and E_γ, we have grouped the data per nucleus in five energy groups from 0 up to 7 MeV medium energies assigned as 0-2 MeV <1.5>, 2-3 MeV (<2.5>), 3-4 MeV (<3.5>), 5-6 MeV (<5.5>) and 6-7 MeV (<6.5>), respectively. In case of multiple entries in an energy window, an unweighted average value has been taken. Such an energy grouping can be viewed as an energy dependent representation for a particular nucleus keeping the benefit of the original binning. Results for the dependence on the mass A or E_γ are shown in Figs 11 and 12.

The next step was to convert these data into energy-dependent entries grouped into five mean mass groups from 50 to 250. In this way we simulated the energy dependent representation of binned

EGAF data which may give information on the PSF behavior for $E_\gamma \to 0$, providing an important source of information for the upbend formulation. The results are shown in Figs 11-12.

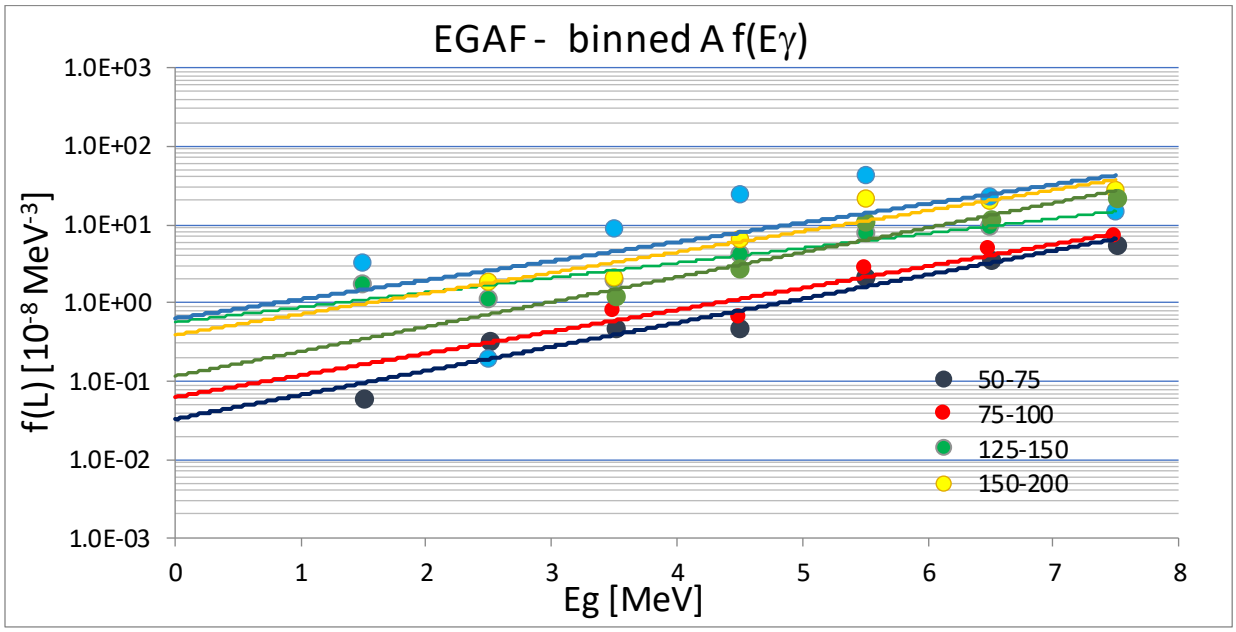

FIG. 11. Grouped EGAF E1 data plotted as a function of the energy E_γ. The trend curves follow a smooth dependence with the increasing A. Note the extrapolated values at $E_\gamma \to 0$ which can be attributed to the upbend tail of the statistical model. Data with A < 50 are not included because of the DC dominance. Exponential fits are shown by solid lines.

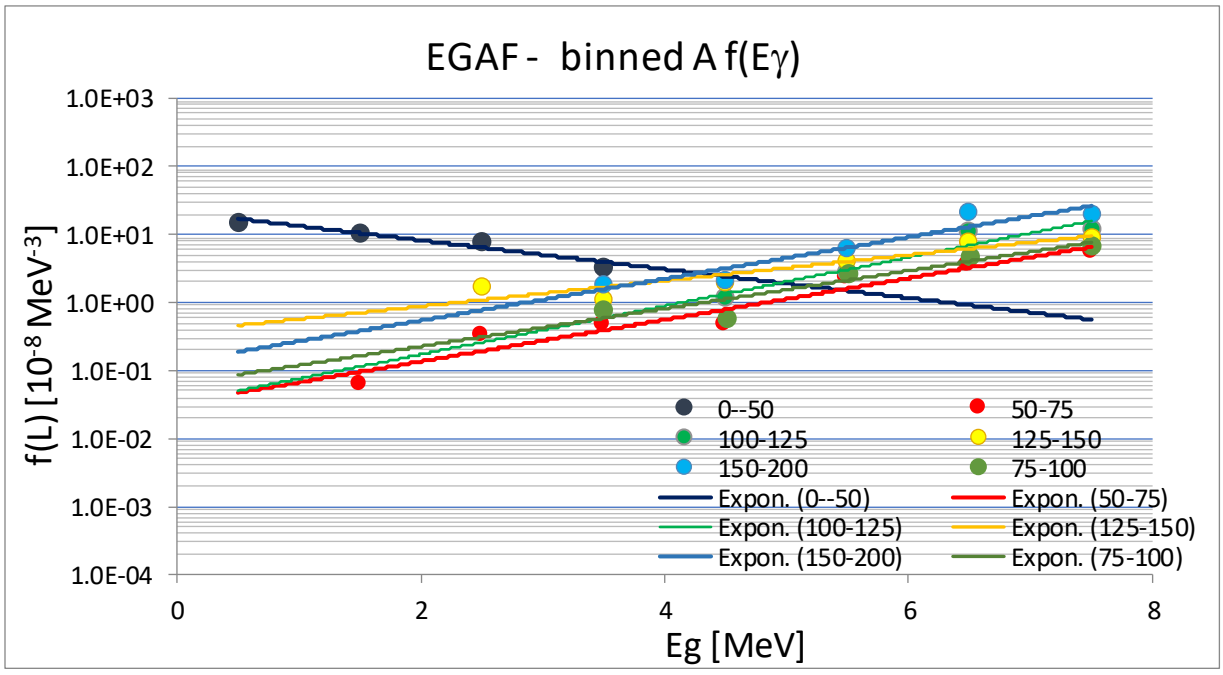

FIG. 12. Same as in Fig.11, but the DC data for A≤50 targets are binned in four energy groups. Exponential fits are shown by solid lines.

An empirical conclusion may be given for the $E_\gamma \rightarrow 0$ limit of the PSF extracted from the trend projections in Fig. 11 for many nuclides (except for targets with $A < 50$). The zero limit $f_{E1}(E_\gamma=0)$ represented mainly by the $<E_\gamma>$=1.5MeV bin scatters around the (0.05 – 3) 10^{-8} MeV^{-3} range on the basis of the linear projection of the grouped EGAF data for nuclides with $A \geq 50$ (see Fig. 12). This behavior is enhanced for light nuclides by the DC processes. To estimate this enhancement accurately, all adopted partial data for $A < 50$ below 4 MeV (from Table 1) have been binned in 4 energy groups as shown in Fig.12. The corresponding trend curve (dark blue) represents the DC component and demonstrates again its dominance against the statistical data.

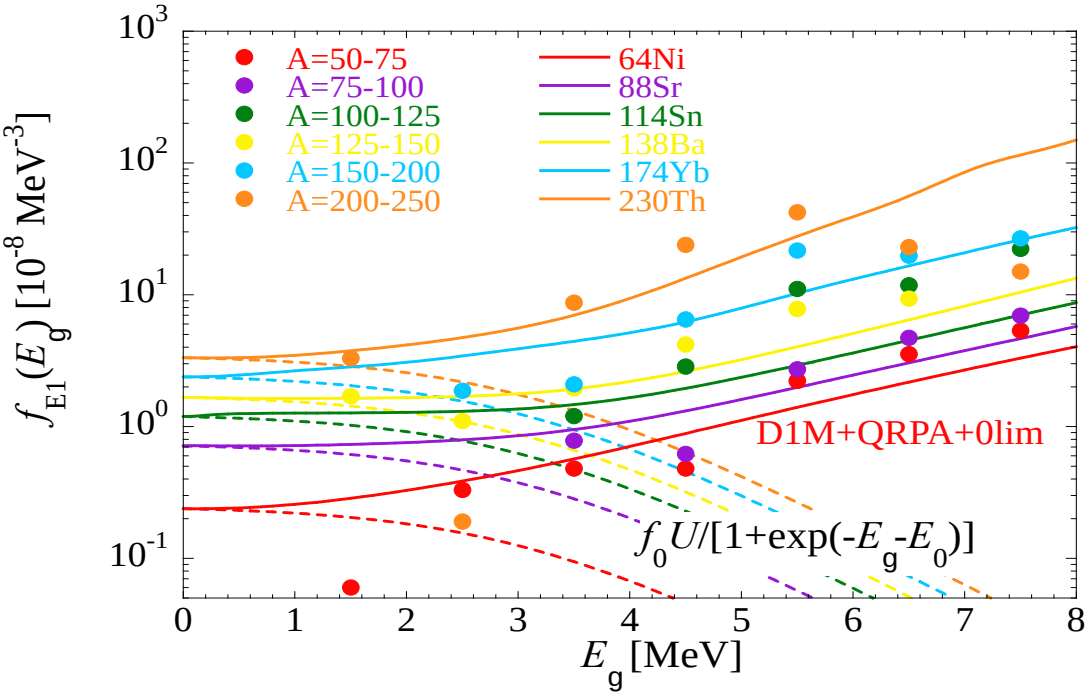

FIG. 13. *Grouped EGAF E1 data (circles) as a function of the energy E_γ. The upbend expression f_{E1}(0lim) based on Eq. (2) (dashed lines) is shown for an average A value in each of the mass bins. The solid lines represent the corresponding D1M+QRPA+0lim predictions with the newly determined f_{E1}(0lim) for specific nuclei within each mass bin. A value of U=5 MeV is adopted in all estimates of f_{E1}(0lim).*

If we use the upbend formulation given by Eq. 1 in Ref. [1], where the values of f_0=$10^{-10}$$MeV^{-4}$ and E_0=3 MeV were proposed based on the SM calculations, an improved determination of these parameters can be extracted from the THC data as illustrated in Fig. 11. If we consider an average value of the neutron binding energy of 5 MeV and take advantage of the $<E_\gamma>$=1.5MeV bin, we can extract the f_0 parameter, at least for A>50 nuclei, with the simple expression

$$f_0 = (0.02A^{-1})/5\ 10^{-8}\ MeV^{-4}. \quad (2)$$

The resulting upbend functional $f_{E1}(0lim) = f_0 U/([1+\exp(-E_\gamma-E_0)]$ is shown in Fig.13 for the average A value in each of the mass bin together with THC data. It describes the lowest energy bin around 1.5 MeV relatively well. Assuming the D1M+QRPA (without the upbend component) predictions

reproduce the E_γ>4 MeV data (Refs [1,2]), it can be inferred that the new determination of the upbend expression (2) improves the overall description of the E1 PSF within the whole nuclear chart. Expression (2) is clearly valid only for A>50, so that a minimum value of f_0~10^{-10} MeV^{-4} should be imposed for light species.

2.5. Conclusions for the E1 strength

The neutron thermal capture data for PSF applications have recently been thoroughly investigated and presented in three INDC reports (Refs [3-5]). The main objective was to ascertain whether any trustworthy low-energy E1 thermal capture data exist and, in addition, whether data trend conclusions can be made from the lowest detected transitions and then used to extract an upbend formulation. The recent conclusions and observations on E1 behavior can be summarized as

1. There is strong evidence that for low-mass targets (A < 45), direct capture data account for the majority of the E1 decay strength. This information, underlined by the DC model, should be considered in the upbend component. However, it is noted that this conclusion applies only for thermal neutron captures. The presence of the DC model will be diminished with increasing incident energies by the dominant presence of the resonance capture.

2. For targets with A > 50 the thermal capture low-energy primary transitions are rarely present except for the actinide isotopes of Th, U and Pu, which have extremely low neutron binding energies. However, for E1 transitions, we efficiently explored the data trend towards the 0lim region and empirically established that the E1 PSF at E_γ = 0 in the range between (0.05 – 3) 10^{-8} MeV^{-3} has a small mass A dependence as given by Eq. (2).

3. Several earlier models, such as GLO, EGLO or SMLO, introduce a non-zero f_{E1} limit for transition energies E_γ tending to zero. The empirical limit, introduced in Ref. [1], is a purely phenomenological upbend, based on two external sources, the experimental data of the Oslo group and the SM calculations. This upbend component has been applied to the D1M+QRPA calculation.

4. The present E1 results from THC data allowed us to further improve the upbend expression suggested in Ref. [1] by introducing a mass dependence in the expression of the f_0 parameter and renormalizing its value with the lowest energy bins available.

3. M1 radiation

The M1 radiation mode substantially differs from the E1 because the adopted collective excitation models (Spin flip and scissors mode) are located below the neutron binding energy and influenced by deformation. Another relevant difference is that despite some observation of the nonstatistical behavior of M1 radiation (see examples in Refs [27, 28]), the contribution of nonstatistical excitations to the decay strength is believed to be negligible. The above-described successful E1 campaign has been repeated for the M1 analysis.

3.1. Database for A < 70 nuclides

First, we reviewed the available data in the low-mass region with A < 70 for using the present THC entries and, if needed, complemented with EGAF sources in the partial PSF format (processed in this work). The listing of addressed data is shown in Table 2. The main weight is again expected

from low-energy transitions indicating most accurately the zero-limit behavior as $E_\gamma \rightarrow 0$. An example of the M1 data is given in Fig. 14 for ^{20}F.

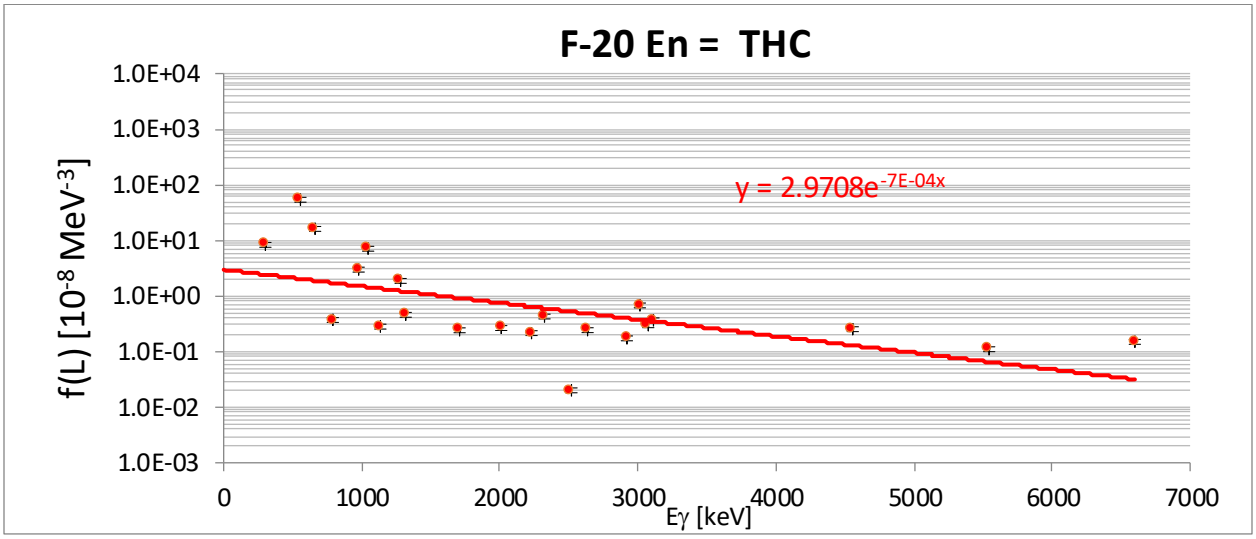

FIG. 14. M1 PSF data from the ^{19}F(n,γ)^{20}F reaction plotted together with an exponentially decreasing trend describing the zero-limit upbend. Note the smoothly increasing strength towards $E_\gamma \rightarrow 0$. A similar feature is found for all studied nuclides.

TABLE 2. List of recommended M1 thermal capture data with $A < 70$ from the THC and EGAF data sources. The last column gives the zero-limit intercept at E_γ=0 value, derived from all data points. No entry indicates the disregarded trend (data shortage) and the value in brackets stands for a too narrow E_γ group. For a detailed overview, it is recommended to download the database from the *M1THC70* link (Ref [29]).

EGAF/PGAA	**THC**	**EGAF** processed in this work	**Recommended sources**	**0lim trend M1** Recommended for visual analysis	$f_{M1}(E_\gamma = 0)$ [10^{-8} MeV^{-3}] Exponential fit → 0lim
F-20	+		THC		2.97
Na-24	+		THC	+	4.7
Mg-25	+		THC	+	1.12
Mg-26	+	+	THC+ EGAF		1.28
Mg-27	+		THC		3.55
Al-28	+		THC	+	22.5
Si-29	+	+	EGAF	+	0.18
Si-30	+	+	EGAF	+	1.59
P-32	+		THC	+	9.09
S-33	+	+	EGAF	+	0.27
S-34	+	+	THC+ EGAF	+	0.49
S-35	+		THC		
Cl-36	+		THC	+	0.67
Cl-38	+		THC		
K-40	+		THC	+	12.29
Ar-41		+	EGAF		

EGAF/PGAA	**THC**	**EGAF** processed in this work	**Recommended sources**	**0lim trend M1** Recommended for visual analysis	$f_{M1}(E_\gamma = 0)$ [10^{-8} MeV^{-3}] Exponential fit → 0lim
K-41		+	Not used		
Ca-41	+		THC		14.54
K-42		+	EGAF	+	1.71
Ca-45		+	EGAF		
Sc-46	+		THC		2.52
Ti-49	+		THC		3.02
Ti-50		+	EGAF		12.75
V-51	+		THC		
Cr-51	+		THC		
V-52	+		THC		6.89
Cr-55		+	EGAF		
Mn-56		+	EGAF		
Fe-57	+		THC		1.15
Fe-59		+	EGAF		(0.08)
Ni-59	+		EGAF		1.69
Co-60	+	+	THC+ EGAF		2.47
Ni-61	+	+	THC+ EGAF		32.77
Ni-63	+	+	EGAF		
Cu-64	+		THC		33.18
Ni-65		+	EGAF		(0.07)
Zn-65	+		THC		
Cu-66	+		THC		15.88
Zn-68	+		THC		

The adopted trend projection of the $E_\gamma \rightarrow 0$ values are given in the last column of Table 2 and are plotted in Fig. 15. The resulting $E_\gamma = 0$ values vary uncertainties due to differences in the number of data points and the width of the E_γ energy region. The scatter in Fig.3 is due to the Porter-Thomas fluctuations, but the fitted trend still gives a reasonable description of the mean $\langle PSF \rangle_{0lim}$ value and its spread. With mass A, a weak increase is observed and can be described by $\langle PSF \rangle_{0lim} = 0.00133\ A^{1.5}$.

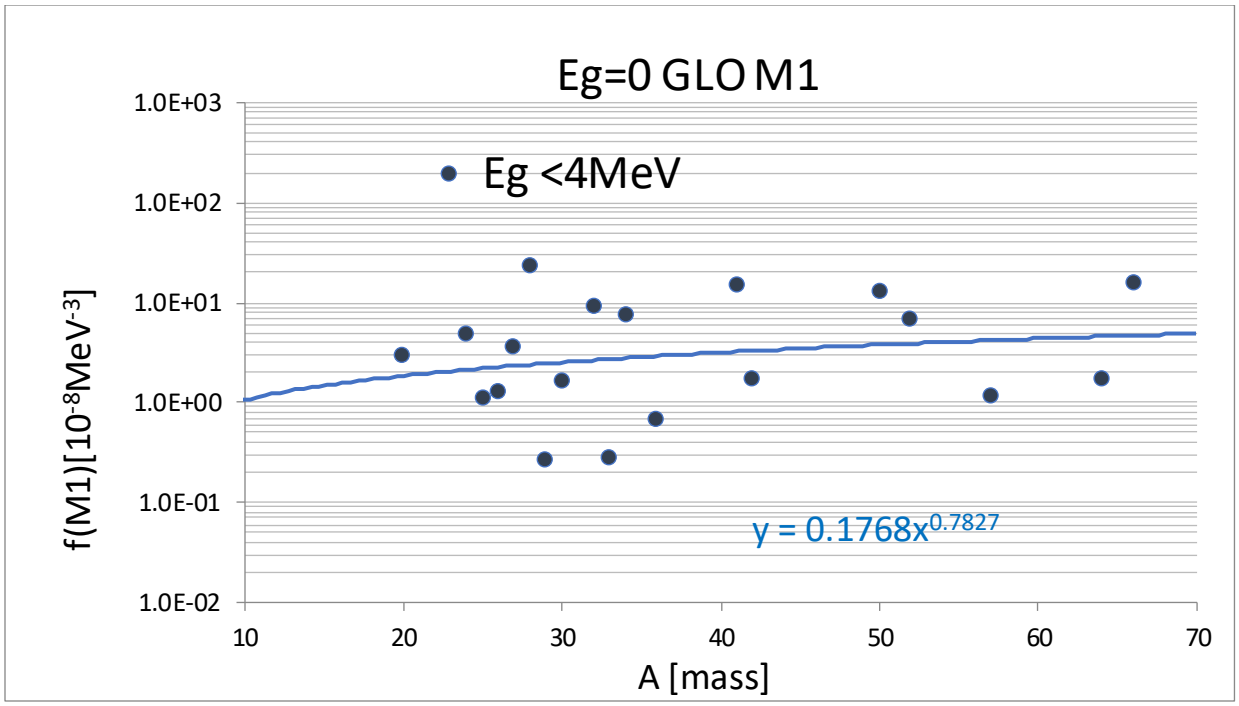

FIG. 15. Adopted M1 PSF at $E_\gamma = 0$ extracted from the exponential trend analysis of the M1 THC partial data for targets with $A < 70$.

3.2. Binned data for A > 70 nuclides

The same processing as for the E1 data has been repeated for M1transitions. The $\langle PSF \rangle_{EGAF}$ data were grouped in the similar six E_γ windows, namely <1.5>=0-2 MeV, <2.5>= 2-3 MeV, <3.5>=3-5 MeV, <5.5>=5-6 MeV, <6.5>=6-7 MeV and <7.5> ≥ 7 MeV. The resulting PSFs are plotted in Fig. 16. The first two groups are plotted as large data points, to indicate data which may strongly influence the $E_\gamma \rightarrow 0$ behavior. The low-energy data ($E_\gamma < 3$ MeV) are present only for $A < 70$ targets (with two exceptions at the mass 131 and 210). The M1 PSF trend is found to increase with $E_\gamma \rightarrow 0$ for all masses and is mainly formed by tails of the spin-flip and scissors mode resonances. It is only slightly dependent on the target deformation and allows us to adjust the upbend in the lowest energy region. In the case of the M1 mode, the non-statistical component remains negligible, so that the rise of the M1 strength for energies $E_\gamma \rightarrow 0$ is well present in the PSF in contrast to the E1 case.

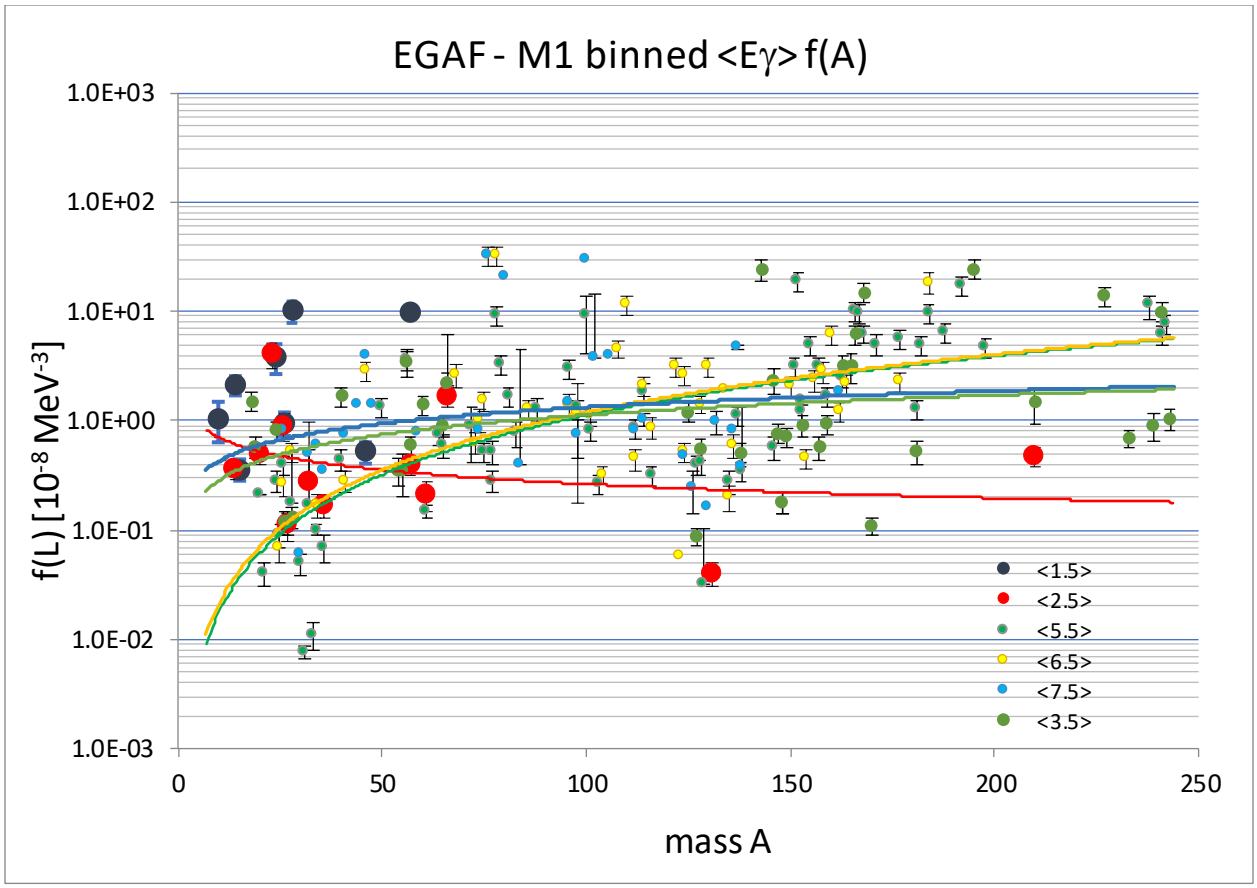

FIG. 16. Grouped EGAF data as a function of mass A for different energy groups. The mean energies <E_γ> are given in the right corner. The plotted trend curves serve as a guiding average. Note that the 1.5 and 2.5 MeV groups (dark blue and red points) data are present only for A < 50 nuclides. The extension of the <2.5> curve above A ~ 100 is due to two data points at A=131 and 210.

The next step was the conversion of these energy-dependent data into five mean mass groups from 50 to 250, similar as the binning made for E1 transitions (see Sect. 2.4). The results are shown in Fig. 17. An empirical conclusion may again be proposed for the PSF $E_\gamma \rightarrow 0$ limit extracted from the trend projections in Fig. 16 except targets with $A > 250$. The derived PSF at E_γ=0 values scatter around 2 10^{-8} MeV^{-3} within the range of (1 - 10) 10^{-8} MeV^{-3} based on the linear projection of data for nuclides with $A \leq 200$. The trend above A = 200 should not be considered due to the limited amount of data, as can be seen in Fig. 16.

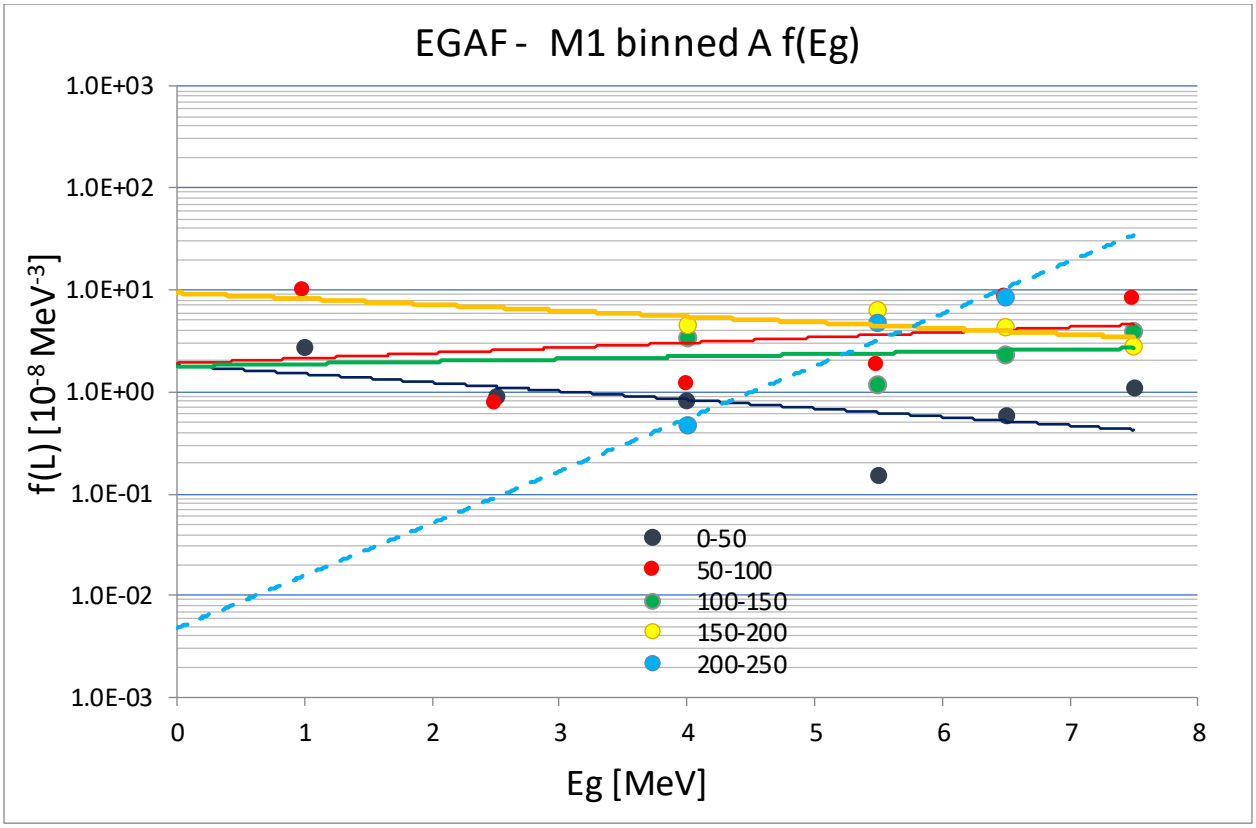

FIG. 17. Grouped EGAF M1 data plotted as a function of the energy E_γ. Note the extrapolated outlier of the A = 200-250 curve is not considered (see text). The best value is probably in the middle of the (1 – 10) 10^{-8} MeV^3 range.

Because the smooth shape of the M1 PSF, the trend analysis using the partial data can also be applied for $A > 70$ targets and be combined with $A < 70$ results. All data analyzed in this work have been considered, altogether 38 nuclides with masses $20 \leq A \leq 233$. The correctness of the fitting procedure depends on the low-energy point E_γ (low), the width of the energy window and the amount of included data points. If E_γ(low) is about 5 MeV or more, the extrapolation for the $E_\gamma \rightarrow 0$ limit becomes dubious, even if many data points are available. The dispersion of the *f*(M1) values above $A \geq 70$ masses is rising and, at $A \sim 150$, the trend towards the zero limit starts to be inaccurate and therefore is not included here. The results of this analysis are shown in Fig. 18. The data for two different E_γ regions look reasonable with a slightly increased trend for the high-energy transitions, which is caused by the fitting procedure. Additionally, the collective M1 (spin-flip, scissors mode) excitations are present throughout all masses, with some variations depending on nuclear deformation.

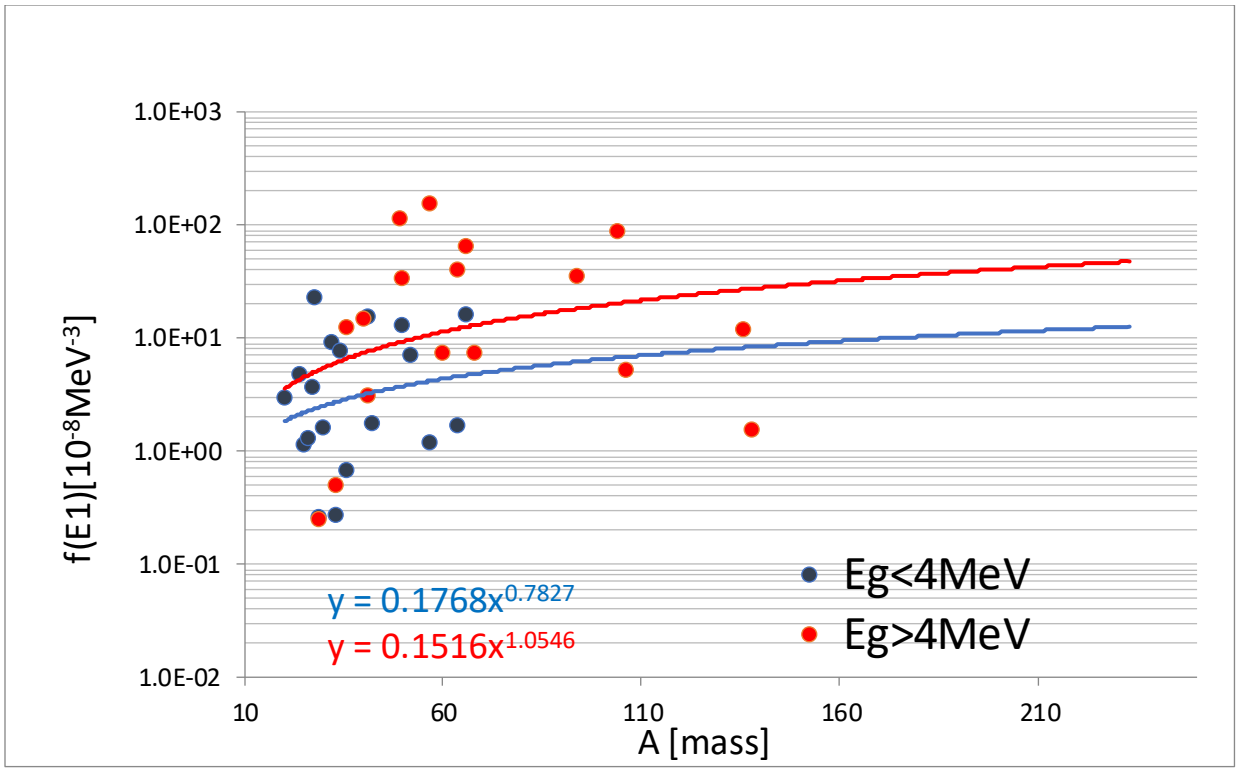

FIG. 18. The adopted PSF values at $E_\gamma = 0$ extracted from the exponential trend analysis of the M1 thermal capture partial data for targets with 20 < A < 233. The data are divided into two energy groups below and above 4 MeV, shown as blue and red data points. Note the missing data above A ~ 150, explained in the text.

Finally, all present approaches point towards the same information, namely a mean $\langle f_{M1}(E_\gamma=0)\rangle$ value of the M1 PSF at zero energy in the (1 - 10) 10^{-8} MeV^{-3} range. It is then justified to use such THC data for the normalization of the M1 upbend formulation and to check the validity of the theoretical PSF in this energy region. More specifically, the M1 upbend has been empirically expressed as (Refs [1,2])

$$f_{M1}(0\text{lim}) = C\ e^{-\eta E_\gamma}$$

where η=0.8MeV^{-1} and C=10^{-8} MeV^{-3} for all nuclei with $A \geq 105$ and C =3 10^{-8} exp (-4β_2) MeV^{-3} for lighter nuclei (where β_2 is the quadrupole deformation parameter). Such values for C, i.e., for the E_γ= 0 limit of the M1 PSF, are seen to be compatible with the present THC estimates (see Fig. 17). For $A \leq 100$ nuclei, the upbend character of the M1 PSF is clearly visible for energies $E_\gamma \leq 2.5$ MeV. Interestingly, when comparing the E1 and M1 strength in the E_γ=0 limit, as can be seen from Figs 13 and 17, the E1 PSF is about a factor of 3 to 10 smaller than the M1 PSF, for light A ≤ 100 nuclei.

3.3. Conclusions for the M1 strength

The main objective was to review the low-energy thermal M1 capture data and used them to update and improve the existing upbend formulation. The recent conclusions and observations on the M1 behavior can be summarized as

1. There is strong evidence that the M1 strength has a smooth increasing trend with decreasing gamma-ray energy for all targets with $A < 250$. The collective M1 (spin-flip, scissors mode) excitations and their variation with nuclear deformation are hidden within the Porter-Thomas data dispersion.

2. For targets with $A > 70$ the low-energy M1 THC transitions are less present. However, we explored efficiently the data trend from light A targets to establish the $E_\gamma \rightarrow 0$ limit of the M1 PSF for all targets up to $A \sim 250$ to range between (1-10) 10^{-8} MeV^{-3}.

3. The empirical M1 upbend PSF extracted from the shell model calculation and previously proposed in Refs. [1,2], i.e., $f_{M1}(0\text{lim}) = C \exp(-\eta E_\gamma)$, is compatible with THC data.

4. Final remarks

The neutron thermal capture data for PSF applications have recently been thoroughly investigated in three IAEA INDC reports (Refs [3-5]). The present work has been carried out with the aim to investigate the E1 thermal capture data and the underlying modelling of low energy transitions with $E_\gamma \rightarrow 0$. The main objective was to ascertain whether any trustworthy low-energy E1 thermal capture data exist and, in addition, whether data trend conclusions can be made from the lowest detected transitions and then used to extract an upbend formulation. One of the novel conclusions is the information on the M1/E1 strength ratio in the $E_\gamma \rightarrow 0$ region, which has a value of M1/E1 ~ 10.

The results of this study contributed more accurate E1 and M1 upbend formulas, normalized to model free experimental evidence from thermal neutron capture data. As an additional benefit the direct E1 capture has been reviewed and its role in the capture mechanism at thermal incident neutron energies verified.

Acknowledgments

JK and SG are grateful to the IAEA for initiating and supporting this work.

JK expresses his gratitude to his late wife Iska who unflaggingly supported this work.

References

[1] S. Goriely, et al., Phys.Rev. C**98** (2018) 014327.

[2] S. Goriely, et al., R*eference Database for Photon Strength Functions*", Eur. Phys. J. A (2019) 55:172.

[3] J. Kopecky, Photon Strength Functions in Thermal Capture, IAEA report INDC(NDS)-0799, 2020, https://www-nds.iaea.org/publications/indc/indc-nds-0799/

[4] J. Kopecky, Photon Strength Functions in Thermal Capture II, IAEA report INDC(NDS)-0815, 2020, https://www-nds.iaea.org/publications/indc/indc-nds-0815/

[5] J. Kopecky and S. Goriely, *Addendum to IAEA(NDS) reports on the neutron capture photon strength sunctions*, INDC(NDS)-0821, 2020, https://www-nds.iaea.org/publications/indc/indc-nds-0821/
[6] R. Firestone, private communication; https://www-nds.iaea.org/pgaa/egaf.html
[7] K. Sieja, Phys. Rev. Lett. **119** (2017) 052502.
[8] I. Bergqvist, et al., Phys.Rev. **158** (1967) 1049.
[9] J. Kopecky, et al., Phys.Rev. C**95** (2017) 054317.
[10] J. Kopecky, Revision and Update of Experimental Gamma-ray Strength Functions derived from the Discrete Neutron Resonance Capture, IAEA report INDC(NDS)-0772, 2018, https://www-nds.iaea.org/publications/indc/indc-nds-0772/
[11] J. Kopecky and S. Goriely, Strength Functions derived from the Discrete and Average Neutron Resonance Capture, IAEA report INDC(NDS)-0790, July 2019, https://www-nds.iaea.org/publications/indc/indc-nds-0790/
[12] J. Kopecky, A.M.J. Spits and A.M. Lane, Phys.Lett. **49B** (1974) 323.
[13] T.J. Kennett, et al., Z.Phys. A**322** (1985) 121.
[14] S. Raman, et al., Phys.Rev. C**32** (1985) 18.
[15] S. Mughabghab, Non-statistical effects in neutron capture, 3. International School on Neutron Physics, Report JINR-D-3-11787, Jont Inst. For Nuclear Research, Dubna (USSR) 1978.
[16] J. Kopecky and C. Plug, Tables of the (n,γ) (d,p) correlations in the 3s- region, RCN Report (1975), RCN-75-005. [copy available upon request]
[17] S. Mughabghab, Atlas of Neutron Resonances, Elsevier, 2018.
[18] J. Kopecky, *E1THC70*, private communication.
[19] D.M. Brink, Ph.D. thesis, Oxford University, 1955.
[20] S.G. Kadmenskij, et al., Sov. J. Nucl. Phys. **37** (1983) 165.
[21] R.E. Chrien, Proc. of the Vth Int. School on Neutron Physics, Alushta 1987, unpublished.
[22] J. Kopecky and R.E. Chrien, Nucl. Phys. A**468** (1987) 285.
[23] J. Kopecky and M. Uhl, Phys.Rev. C**41** (1990) 1941.
[24] J. Kopecky, M. Uhl and R.E. Chrien, Phys.Rev. C**47** (1993) 312.
[25] T. Belgya, O. Bersillon, R. Capote Noy, et al, , Handbook for calculations of nuclear reaction data, RIPL 2 Reference Input Parameter Library-2,, IAEA-TECDOC-1506, June 2006, https://www.iaea.org/publications/7129/handbook-for-calculations-of-nuclear-reaction-data-ripl-2
[26] S. Goriely and V. Plujko, Phys.Rev. C**99** (2019) 014303.
[27] C.F. Clement, A.M. Lane and J. Kopecky, Phys. Lett. **71B** (1977) 10.
[28] R.E. Chrien and J.Kopecky, Phys.Rev.Lett. **39** (1977) 911.
[29] J. Kopecky, *M1THC70*, private communication.

Nuclear Data Section
International Atomic Energy Agency
Vienna International Centre, P.O. Box 100
A-1400 Vienna, Austria

E-mail: nds.contact-point@iaea.org
Fax: (43-1) 26007
Telephone: (43-1) 2600 21725
Web: http://nds.iaea.org